

# ASYMPTOTIC-PRESERVING SCHEMES FOR THE BOLTZMANN MIXTURE MODEL WITH DISPARATE MASS \*

ZHEN HAO <sup>†</sup>, NING JIANG <sup>‡</sup>, AND LIU LIU <sup>§</sup>

**Abstract.** In this paper, we develop and implement an efficient asymptotic-preserving (AP) scheme to solve the gas mixture of Boltzmann equations, under the so-called “relaxation time scale” relevant to the epochal relaxation phenomenon. The disparity in molecular masses, ranging across several orders of magnitude, leads to significant challenges in both the evaluation of collision operators and designing of efficient numerical schemes in order to capture the multi-scale nature of the dynamics. A direct implementation by using the spectral method faces prohibitive computational costs as the mass ratio decreases due to the need to resolve vastly different thermal velocities. Different from [I. M. Gamba, S. Jin, and L. Liu, *Commun. Math. Sci.*, 17 (2019), pp. 1257–1289], we propose an alternative approach by conducting asymptotic expansions for the collision operators, which can significantly reduce the computational complexity and works well for uniformly small  $\varepsilon$ . By incorporating the separation of three time scales in the model’s relaxation process [P. Degond and B. Lucquin-Desreux, *Math. Models Methods Appl. Sci.*, 6 (1996), pp. 405–436], we design an AP scheme that is able to capture the epochal relaxation phenomenon of disparate mass mixtures while maintaining the computational efficiency. Numerical experiments will demonstrate the effectiveness of our proposed scheme in handling large mass ratios of heavy and light species, in addition to validating the AP properties.

**Key words.** gas mixture, Boltzmann equations, disparate mass, asymptotic analysis for collision operators, asymptotic-preserving scheme

**MSC codes.** 82C40, 65M70, 65T40, 65Y20, 35B25

**1. Introduction.** The numerical computation of gas mixtures with disparate masses is very challenging, with important applications in plasma physics and aerospace engineering. In practice, mass ratios of light and heavy molecules usually span several orders of magnitude, from  $10^2$  to  $10^5$ , as seen in spacecraft re-entry plasma environments [2], ITER fusion reactor dust-plasma interactions [33], and evaporation/condensation processes [34].

In kinetic theory, the Boltzmann equation models the evolution of rarefied gases, with the multi-species Boltzmann equation describing gas mixtures. Major challenges for solving the Boltzmann equation include the non-local collision operator of an integral type and treatment of the multiple scales. Over the decades, deterministic methods, being free of statistical noise, are particularly advantageous for solving the Boltzmann equation, especially in near-continuum flows [11]. In particular, the Fourier spectral method has been popularly used since the pioneer work [28, 29], with fast spectral method developed afterwards, see for examples [13, 15, 16, 27]. For gas mixtures, recent studies have achieved notable progress [21, 35].

---

\*Submitted to arXiv Nov 20, 2024.

**Funding:** Z. Hao acknowledges the computational resource of The Chinese University of Hong Kong during his visit. N. Jiang acknowledges the support by NSFC grants 12371224, 11971360, 11731008 and the Strategic Priority Research Program of Chinese Academy of Sciences grant XDA25010404. L. Liu acknowledges the support by National Key R&D Program of China (2021YFA1001200), Ministry of Science and Technology in China, Early Career Scheme (24301021) and General Research Fund (14303022 & 14301423) funded by Research Grants Council of Hong Kong.

<sup>†</sup>School of Mathematics and Statistics, Wuhan University, Wuhan 430072, P. R. China (zhao\_math@whu.edu.cn).

<sup>‡</sup>School of Mathematics and Statistics, Wuhan University, Wuhan 430072, P. R. China (njiang@whu.edu.cn).

<sup>§</sup>The Chinese University of Hong Kong, Hong Kong (liuliu@math.cuhk.edu.hk).

Compared to single-species or standard multi-species cases, gas mixtures with disparate masses pose substantial computational challenges in handling collision operators. A key characteristic of these mixtures is the large disparity in species’ thermal velocities: the computational domain must accommodate the fastest species, while grid spacing must resolve the slowest. As a result, direct implementations of spectral methods would have a computational complexity that scales with the mass ratio [21, 35]. Various studies address these challenges through adaptive meshing in velocity space [32] and asymptotic models tailored to large mass ratios [6, 32].

Besides the computational challenges for the nonlinear collision operators, the dynamics of the gas mixture leads to a more complex physics. We distinguish the “heavy” species (denoted by ‘H’) and the “light” species (denoted by ‘L’). Define the square-rooted mass ratio between these two species:  $\varepsilon = \sqrt{m^L/m^H}$ , and the disparate mass regime refers to the case when  $\varepsilon \ll 1$ . Back in the 1960s, the epochal relaxation phenomenon was first pointed out by Grad [20], who noticed that the relaxation rate of the light species is faster than that of the heavy species. There has been several work along this line, see [1, 7, 9, 19, 26, 30, 31]. In particular, Degond and Lucquin-Desreux [8–10] characterized the relaxation process in binary gas mixtures through a separation of three time-scales and derived their corresponding asymptotic limits. Under the longest time scale, both particle distributions reach thermal equilibrium, with their temperatures evolving toward each other which is governed by a relaxation equation. This is the asymptotic regime we are particularly interested in this work.

With the distinctive stiffness in our model (2.3) under the above-mentioned longest time scale, designing an efficient asymptotic-preserving (AP) scheme becomes a challenging task, especially in the disparate mass case when  $\varepsilon \ll 1$ . The goal of Asymptotic-Preserving (AP) schemes [23] is to avoid resolving the small scaling parameter numerically while preserving the macroscopic behavior of the model at the discretized level. Several AP schemes have been designed for the Boltzmann mixture model, for examples see [24, 25]. However, none of those work considered the particular time scalings for the disparate mass models as we focus on in this work.

We mention that in [17], the authors studied the same model and employed the ansatzes  $f^{L,H} = f_0^{L,H} + \varepsilon f_1^{L,H}$  to design a system for four variables  $f_0^{L,H}, f_1^{L,H}$ ; they only gave a theoretical proof that the numerical method was AP but fail to carry out implementations, given their scheme was overly complicated and seemed computationally infeasible in practice.

**Novelty and contributions:** Compared to this earlier work [17], we propose a significantly simpler and novel numerical approach. To the best of our knowledge, this current work is the *first* to provide an efficient, computationally cheap AP scheme that can accurately capture the “epochal relaxation” phenomenon for the Boltzmann mixture model with disparate mass, yet without suffering the computational cost even if  $\varepsilon \ll 1$ . Numerical results have demonstrated the feasibility and effectiveness of our new method.

Besides, another main novelty of our work lies in the efficient computation of inter-particle collision operators. In [9], the authors derived the scaling of equations as a function of the mass ratio of the particle, expanded the collision operators in powers of the mass ratio and showed the dynamics of the mixtures at various time scales. Inspired by but different from that theoretical work, we mainly contribute in the following aspects: (i) Our expansion is different from [9] since we incorporate a lower-order collision operator term ( $Q_2$ ) to account for the slowest time scale. (ii) Another key contribution is the efficient evaluation of angular integrals for the new

operators after expansion, while ensuring its compatibility with the Cartesian grid for the convenience of computing distribution functions. This requires a carefully designed grid layout and utilizing the interpolation, which ensures the accuracy of calculations. This approach significantly reduces the computational costs compared to straightforward spectral type methods, achieving a *uniform* efficiency even when the mass ratio is extremely small. (iii) Lastly, employing the BGK-penalty idea first introduced by [12] for the single-species Boltzmann equation, our designed numerical scheme satisfies the AP property, is able to accurately capture the epochal relaxation in the disparate mass regime and maintains a consistent efficiency.

The rest of the paper is organized as the following: Section 2 introduces the gas mixture of Boltzmann equation under different time scales and reviews its key properties in the disparate mass regime. Section 3 carries out asymptotic approximations for the inter-particle collision operators, introduces our carefully designed asymptotic-expansion method and compares the computational efficiency with the standard spectral approach. In Section 4, we present the AP time discretization and its theoretical analysis. In Section 5, we show the robustness and efficiency of our proposed AP scheme in the numerical examples, comparing with the brutal-force spectral method and the time evolution of macroscopic quantities solved by the relaxation model when  $\varepsilon$  is small. Lastly, we conclude the paper in Section 6.

**2. The disparate-mass gas mixture model.** In this section, we first introduce the Boltzmann equations for gas mixtures and review the three different time scalings discussed in [9]. Then we will focus on the so-called “epochal relaxation” by considering the slowest time scale, and derive its macroscopic model as the scaling parameter (square-root of mass ratio) goes to zero.

**2.1. The Boltzmann equation for gas mixture.** The time evolution of the distribution functions of a binary gas mixture due to collisions is given by the two-species equations:

$$\begin{aligned}\partial_t f^\alpha &= Q^{\alpha\alpha}(f^\alpha, f^\alpha) + Q^{\alpha\beta}(f^\alpha, f^\beta), \\ \partial_t f^\beta &= Q^{\beta\beta}(f^\beta, f^\beta) + Q^{\beta\alpha}(f^\beta, f^\alpha),\end{aligned}$$

where  $f^\alpha$  and  $f^\beta$  are the distribution functions of the species  $\alpha$  and  $\beta$ . Here,  $Q^{\alpha\alpha}$  and  $Q^{\beta\beta}$  denote collisions within the same species, while  $Q^{\alpha\beta}$  and  $Q^{\beta\alpha}$  denote collisions between different species. We refer to these as “intra-particle” and “inter-particle” collisions, respectively.

The Boltzmann collision operator in velocity space of dimension  $d_v$  is given by [3, 5]

$$Q^{\alpha\beta}(f^\alpha, f^\beta)(v^\alpha) = \int_{\mathbb{R}^{d_v} \times \mathbb{S}^{d_v-1}} B^{\alpha\beta}(|v^\alpha - v^\beta|, \sigma)(f'^\alpha f'^\beta - f^\alpha f^\beta) d\sigma dv^\beta,$$

where  $f'^\alpha = f^\alpha(v'^\alpha)$ ,  $f'^\beta = f^\beta(v'^\beta)$ ,  $f^\alpha = f^\alpha(v^\alpha)$ , and  $f^\beta = f^\beta(v^\beta)$ . The velocities  $v^\alpha$  and  $v^\beta$  are the pre-collision velocities of species  $\alpha$  and  $\beta$ , whereas  $v'^\alpha$  and  $v'^\beta$  are their post-collision velocities. Throughout this work, we omit superscripts on velocities when unambiguous. The post-collision velocities can be parameterized through the collision transform

$$\begin{aligned}v'^\alpha &= \frac{m^\alpha v^\alpha + m^\beta v^\beta}{m^\alpha + m^\beta} + \frac{m^\beta}{m^\alpha + m^\beta} |v^\alpha - v^\beta| \sigma, \\ v'^\beta &= \frac{m^\alpha v^\alpha + m^\beta v^\beta}{m^\alpha + m^\beta} - \frac{m^\alpha}{m^\alpha + m^\beta} |v^\alpha - v^\beta| \sigma,\end{aligned}$$

with  $m^\alpha$  and  $m^\beta$  representing the mass of species  $\alpha$  and  $\beta$  and  $\sigma$  being a vector ranging over the unit sphere  $\mathbb{S}^{d_v-1}$ . The collision kernel  $B$  that associates with the cross-section  $\Sigma$  is defined by

$$B^{\alpha\beta}(|v^\alpha - v^\beta|, \sigma) = |v^\alpha - v^\beta| \Sigma^{\alpha\beta}.$$

In general,  $\Sigma^{\alpha\beta}$  depends on the relative energy and the scattering angle [8]

$$\Sigma^{\alpha\beta} = \Sigma^{\alpha\beta} \left( \mu^{\alpha\beta} |v^\alpha - v^\beta|^2, \sigma \cdot \frac{v^\alpha - v^\beta}{|v^\alpha - v^\beta|} \right),$$

with  $\mu^{\alpha\beta} = \frac{m^\alpha m^\beta}{m^\alpha + m^\beta}$  defined as the reduced mass. The properties of these collision operators are crucial to study the long time behavior of the solutions and derive the asymptotic models. We briefly review them in the following [3, 4]

**PROPOSITION 2.1 (Properties of the collision operators).**

- *Conservation of mass, total momentum and total energy:*

$$\begin{aligned} \int_{\mathbb{R}^{d_v}} Q^{\alpha\alpha} dv &= 0, & \int_{\mathbb{R}^{d_v}} Q^{\alpha\beta} dv &= 0. \\ \int_{\mathbb{R}^{d_v}} Q^{\alpha\alpha} m^\alpha v dv &= 0, & \int_{\mathbb{R}^{d_v}} Q^{\alpha\beta} m^\alpha v + Q^{\beta\alpha} m^\beta v dv &= 0. \\ \int_{\mathbb{R}^{d_v}} Q^{\alpha\alpha} m^\alpha |v|^2 dv &= 0, & \int_{\mathbb{R}^{d_v}} Q^{\alpha\beta} m^\alpha |v|^2 + Q^{\beta\alpha} m^\beta |v|^2 dv &= 0. \end{aligned}$$

- *Thermal equilibria:*

$$(2.1) \quad Q^{\alpha\alpha}(f^\alpha, f^\alpha) = 0 \iff f^\alpha = M^\alpha(v),$$

where the Maxwellian distribution is defined as

$$M^\alpha(v) = \mathcal{M}_{n^\alpha, u^\alpha, T^\alpha}(v) := \frac{n^\alpha}{\left(\frac{2\pi T^\alpha}{m^\alpha}\right)^{d_v/2}} \exp\left(-\frac{m^\alpha |v - u^\alpha|^2}{2T^\alpha}\right)$$

with density  $n^\alpha$ , mean velocity  $u^\alpha$  and temperature  $T^\alpha$  given by

$$\int_{\mathbb{R}^{d_v}} f^\alpha(v) \begin{pmatrix} 1 \\ m^\alpha v \\ m^\alpha |v|^2 \end{pmatrix} dv = \begin{pmatrix} n^\alpha \\ m^\alpha n^\alpha u^\alpha \\ m^\alpha n^\alpha |u^\alpha|^2 + d_v T^\alpha \end{pmatrix}.$$

The same property holds for  $Q^{\beta\beta}(f^\beta, f^\beta)$ .

- *If the pair  $f^\alpha$  and  $f^\beta$  satisfy*

$$Q^{\alpha\alpha}(f^\alpha, f^\alpha) + Q^{\alpha\beta}(f^\alpha, f^\beta) = 0, \quad Q^{\beta\beta}(f^\beta, f^\beta) + Q^{\beta\alpha}(f^\beta, f^\alpha) = 0,$$

then  $f^\alpha$  and  $f^\beta$  are two Maxwellians with the same mean velocity  $u$  and temperature  $T$ , namely

$$f^\alpha = \mathcal{M}_{n^\alpha, u, T}(v), \quad f^\beta = \mathcal{M}_{n^\beta, u, T}(v).$$

**2.2. Different time scalings.** In this work, we are interested in a binary gas mixture where the masses of the two species are significantly different. Define the square-rooted mass ratio between the light and heavy species by

$$\varepsilon = \sqrt{\frac{m^L}{m^H}},$$

The disparate mass regime refers to the case when  $\varepsilon \ll 1$ . The relevant scaling in this regime ([8, 9]) gives

$$(2.2) \quad \begin{aligned} \partial_t f^L &= Q^{LL}(f^L, f^L) + Q_\varepsilon^{LH}(f^L, f^H), \\ \partial_t f^H &= \varepsilon [Q^{HH}(f^H, f^H) + Q_\varepsilon^{HL}(f^H, f^L)]. \end{aligned}$$

According to [9], there are three time scales which are listed in order as follows

- (i) The fastest time scale ( $\hat{t}_0 = t_0$ ): collision time of the light species,
- (ii) The intermediate time scale ( $\hat{t}_0 = t_0/\varepsilon$ ): collision time of the heavy species,
- (iii) The slowest time scale ( $\hat{t}_0 = t_0/\varepsilon^2$ ): temperature relaxation time scale,

where  $t_0$  denotes the time scale in (2.2). This temporal scaling separation is referred as the ‘‘epochal relaxation’’ phenomenon and first pointed out by Grad [20].

In this work, we are interested in the slowest time scale, under which both particle distribution functions are thermalized and the temperatures evolve toward each other via a relaxation equation. By considering this time scale we are able to study thoroughly the whole epochal relaxation phenomenon. Under the above scaling (iii), the Boltzmann mixture model is given by ([8, 9])

$$(2.3) \quad \begin{aligned} \partial_t f^L &= \frac{1}{\varepsilon^2} [Q^{LL}(f^L, f^L) + Q_\varepsilon^{LH}(f^L, f^H)], \\ \partial_t f^H &= \frac{1}{\varepsilon} [Q^{HH}(f^H, f^H) + Q_\varepsilon^{HL}(f^H, f^L)]. \end{aligned}$$

The scaled collision operator between the light and heavy species is given by

$$(2.4) \quad Q_\varepsilon^{LH}(f^L, f^H)(v^L) = \sqrt{1 + \varepsilon^2} \int_{\mathbb{R}^{d_v} \times \mathbb{S}^{d_v-1}} B^{LH} \left( \frac{|g^{LH}|}{\sqrt{1 + \varepsilon^2}}, \sigma \right) (f'^L f'^H - f^L f^H) d\sigma dv^H,$$

with collision rules

$$(2.5) \quad \begin{cases} v'^L = v^L - \frac{1}{1 + \varepsilon^2} g^{LH} + \frac{1}{1 + \varepsilon^2} |g^{LH}| \sigma, \\ \varepsilon v'^H = v^L - \frac{1}{1 + \varepsilon^2} g^{LH} - \frac{\varepsilon^2}{1 + \varepsilon^2} |g^{LH}| \sigma. \end{cases}$$

Similarly, the collision operator between the heavy and light species is defined as

$$(2.6) \quad Q_\varepsilon^{HL}(f^H, f^L)(v^H) = \frac{\sqrt{1 + \varepsilon^2}}{\varepsilon} \int_{\mathbb{R}^{d_v} \times \mathbb{S}^{d_v-1}} B^{HL} \left( \frac{|g^{HL}|}{\sqrt{1 + \varepsilon^2}}, \sigma \right) (f'^H f'^L - f^H f^L) d\sigma dv^L,$$

with collision rules

$$(2.7) \quad \begin{cases} \varepsilon v'^H = \varepsilon v^H - \frac{\varepsilon^2}{1 + \varepsilon^2} g^{HL} + \frac{\varepsilon^2}{1 + \varepsilon^2} |g^{HL}| \sigma, \\ v'^L = \varepsilon v^H - \frac{\varepsilon^2}{1 + \varepsilon^2} g^{HL} - \frac{1}{1 + \varepsilon^2} |g^{HL}| \sigma, \end{cases}$$

where  $g^{LH} = v^L - \varepsilon v^H = -g^{HL}$  denotes the relative velocity.

We summarize the properties of the scaled collision operators below.

PROPOSITION 2.2 (**Conservation properties of the scaled collision operators**).

$$\begin{aligned} \int_{\mathbb{R}^{d_v}} Q_\varepsilon^{LH} dv &= 0, & \int_{\mathbb{R}^{d_v}} Q_\varepsilon^{HL} dv &= 0, \\ \int_{\mathbb{R}^{d_v}} Q_\varepsilon^{LH} v + Q_\varepsilon^{HL} v dv &= 0, \\ \int_{\mathbb{R}^{d_v}} Q_\varepsilon^{LH} |v|^2 + \varepsilon Q_\varepsilon^{HL} |v|^2 dv &= 0. \end{aligned}$$

This corresponds to conservation of mass, total momentum and energy for the scaled collision operators.

**2.3. Epochal relaxation and the macroscopic model.** In a series of work by Degond and Lucquin-Desreux [9, 10], an asymptotic analysis based on expansions of the inter-particle collision operators are shown, and it provides a concrete picture of the three-time scale separations (epochal relaxation phenomenon). Here we only review the macroscopic model under the slowest time scale.

In the slowest time scale ( $\hat{t}_0 = t_0/\varepsilon^2$ ), there exists  $n^L, n^H \geq 0$ ,  $u^H \in \mathbb{R}^{d_v}$  and  $T^L, T^H \geq 0$  such that

$$f_\varepsilon^L = \mathcal{M}_{n^L, 0, T^L}, \quad f_\varepsilon^H = \mathcal{M}_{n^H, u^H, T^H}.$$

Here the temperatures ( $T^L(t), T^H(t)$ ) satisfy the following relaxation equations:

$$(2.8) \quad \begin{cases} \frac{d}{dt} \left( \frac{d_v n^L T^L}{2} \right) = -d_v \frac{\lambda(T^L)}{T^L} n^H (T^L - T^H), \\ \frac{d}{dt} \left( \frac{d_v n^H T^H}{2} \right) = -d_v \frac{\lambda(T^L)}{T^L} n^H (T^H - T^L), \end{cases}$$

where  $\lambda(T)$  is given by

$$\lambda(T) = \frac{2}{d_v} \int_{\mathbb{R}^{d_v}} \int_{\mathbb{S}^{d_v-1}} B^{LH}(|v|, \sigma) |v|^2 \mathcal{M}_{n^L, 0, T^L} d\sigma dv$$

**2.4. Asymptotic analysis of inter-particle collision operators.** In addition to deriving macroscopic equations, the asymptotic analysis of inter-particle collision operators could also provide us with efficient surrogate operators in numerical implementation for the original collision operators with scalings. We briefly review the study in [8–10]. The difference is that we present here using the  $\sigma$ -representation instead of  $\Omega$ -representations in the literature, since it will be more convenient for numerical computation.

THEOREM 2.3 (**Asymptotic expansion of collision operators**). *Let  $f^L(v)$  and  $f^H(v)$  be sufficiently smooth functions. Then we have*

$$(2.9) \quad \begin{aligned} Q_\varepsilon^{LH} &= \sqrt{1 + \varepsilon^2} (Q_0^{LH} + \varepsilon Q_1^{LH} + \mathcal{O}(\varepsilon^2)), \\ Q_\varepsilon^{HL} &= \sqrt{1 + \varepsilon^2} (Q_0^{HL} + \varepsilon Q_1^{HL} + \mathcal{O}(\varepsilon^2)). \end{aligned}$$

These asymptotic operators ( $Q_0, Q_1$ ) own the following properties:

1. For any function  $f^H$ , we have

- (a) If  $f^L$  is a function of  $|v^L|$ , then  $Q_0^{LH}(f^L, f^H) = 0$ ,  
 (b) If  $f^L$  is an even function, then  $Q_0^{HL}(f^H, f^L) = 0$ .
2. Conservation properties:

$$\begin{aligned} \int_{\mathbb{R}^{d_v}} Q_i^{LH} dv &= \int_{\mathbb{R}^{d_v}} Q_i^{HL} dv = 0, \quad i \geq 0, \\ \int_{\mathbb{R}^{d_v}} Q_i^{LH} v + Q_i^{HL} v dv &= 0, \quad i \geq 0, \\ \int_{\mathbb{R}^{d_v}} Q_i^{LH} |v|^2 + Q_{i-1}^{HL} |v|^2 dv &= 0, \quad i \geq 1, \\ \int_{\mathbb{R}^{d_v}} Q_0^{LH} |v|^2 dv &= 0. \end{aligned}$$

**3. Efficient approximations for the inter-particle collision operators.** In this section, we will discuss the numerical implementation of the collision operators. First, notice that the intra-particle collision operators  $Q^{LL}(f^L, f^L)$  and  $Q^{HH}(f^H, f^H)$  are the same as the single-species Boltzmann collision operator. We employ the fast Fourier spectral method in Mouhot-Pareschi [27], which has a computational complexity of  $\mathcal{O}(N_v^{d_v} \log N_v)$ , where  $N_v$  denotes the number of points used in the velocity discretization.

The numerical implementation of the inter-particle collision operators is complicated by the non-unitary mass ratio between different molecular particles. In this regard, the fast spectral methods by [21, 35] achieve a computational complexity of  $\mathcal{O}(N_v^{d_v+1} \log N_v)$ . However, directly applying those methods to  $Q_\varepsilon^{LH}(f^L, f^H)$  and  $Q_\varepsilon^{HL}(f^H, f^L)$ , especially in disparate mass regimes ( $\varepsilon \ll 1$ ), does not work well. According to [21, 35], the spectral methods are not specifically designed for systems with large mass disparities. Direct numerical implementation in such regimes requires the computational cost increasing in the order of  $\mathcal{O}(1/\varepsilon)$ .

On the other hand, the scaling of the inter-particle collision operators here is different from those in [21, 35]. Recall the collision rules (2.5) of the inter-particle collision operators given by

$$\begin{cases} v'^L = v^L - \frac{v^L - \varepsilon v^H}{1 + \varepsilon^2} + \frac{|v^L - \varepsilon v^H| \sigma}{1 + \varepsilon^2}, \\ \varepsilon v'^H = v^L - \frac{v^L - \varepsilon v^H}{1 + \varepsilon^2} - \frac{\varepsilon^2 |v^L - \varepsilon v^H| \sigma}{1 + \varepsilon^2}, \end{cases}$$

we observe that the different scales of  $v^L$  and  $v^H$  inevitably needs some modifications to the standard Fourier spectral approaches. Based on the work by Jaiswal-Alexeenko-Hu [21], we present in Appendix A a modified framework of evaluating the scaled collision operators  $Q_\varepsilon^{LH}(f^L, f^H)$  and  $Q_\varepsilon^{HL}(f^H, f^L)$ .

In this work, we primarily focus on the mixture problem with large mass ratios ( $\varepsilon \ll 1$ ). Instead of exploring more sophisticated spectral methods computationally feasible for small  $\varepsilon$ , our key idea is to utilize the asymptotic expansions (2.9) as efficient approximations for the inter-particle collision operators, which aims to reduce the computational cost significantly while maintaining the accuracy.

**3.1. The asymptotic-expansion (AE) method.** In this section, we present an asymptotic analysis which is slightly different from Theorem 2.3 and [8–10]. When

$\varepsilon \ll 1$ , one can derive the asymptotic expansions for  $Q_\varepsilon^{LH}$  and  $Q_\varepsilon^{HL}$ :

$$\begin{aligned} Q_\varepsilon^{LH} &= \sqrt{1 + \varepsilon^2} (Q_0^{LH} + \varepsilon Q_1^{LH} + \varepsilon^2 Q_2^{LH} + \mathcal{O}(\varepsilon^3)), \\ Q_\varepsilon^{HL} &= \sqrt{1 + \varepsilon^2} (Q_0^{HL} + \varepsilon Q_1^{HL} + \mathcal{O}(\varepsilon^2)). \end{aligned}$$

Our asymptotic expansion (AE) method consists of evaluating  $Q_\varepsilon^{LH}$  and  $Q_\varepsilon^{HL}$  by

$$(3.1) \quad \begin{aligned} Q_{\text{AE}}^{LH} &= \sqrt{1 + \varepsilon^2} (Q_0^{LH} + \varepsilon Q_1^{LH} + \varepsilon^2 Q_2^{LH}), \\ Q_{\text{AE}}^{HL} &= \sqrt{1 + \varepsilon^2} (Q_0^{HL} + \varepsilon Q_1^{HL}), \end{aligned}$$

which brings a loss of accuracy at level  $\mathcal{O}(\varepsilon^2)$ , compared to the original  $Q_\varepsilon^{LH}$  and  $Q_\varepsilon^{HL}$ . In contrast with (2.9), a higher order expansion of  $Q_\varepsilon^{LH}$  that involves  $Q_2^{LH}$  is used. For simplicity, we consider  $d_v = 2$  and constant collision kernels  $B^{LH}$ ,  $B^{HL}$  in our numerical experiments, then the collision operators can be written in the following simplified forms. A sketchy derivation can be found in Appendix B. The light-heavy collision operators for  $v^L \neq 0$  read

$$(3.2) \quad \begin{aligned} Q_0^{LH}(v^L) &= B^{LH} n^H (\langle f^L \rangle - 2\pi f^L), \\ Q_1^{LH}(v^L) &= B^{LH} n^H u^H \cdot (\langle \nabla_{v^L} f^L \rangle - \nabla_{v^L} \langle f^L \rangle), \\ Q_2^{LH}(v^L) &= B^{LH} \left\{ 2n^H \langle f^L \rangle - n^H \frac{v^L}{|v^L|} \cdot \langle \sigma f^L \rangle + n^H |v^L| \langle \sigma \cdot \nabla_{v^L} f^L \rangle \right. \\ &\quad + \left( \frac{1}{2} n^H |u^H|^2 + n^H T^H \right) \frac{1}{|v^L|} \langle \sigma \cdot \nabla_{v^L} f^L \rangle - n^H v^L \cdot \langle \sigma \otimes \sigma \cdot \nabla_{v^L} f^L \rangle \\ &\quad + \frac{1}{2} \int_{\mathbb{R}^2} v^H \otimes v^H f^H dv^H : \left( - \frac{v^L \otimes v^L}{|v^L|^3} \langle \sigma \cdot \nabla_{v^L} f^L \rangle + \langle \nabla_{v^L}^2 f^L \rangle \right. \\ &\quad \left. \left. - 2 \langle \nabla_{v^L}^2 f^L \cdot \sigma \rangle \otimes \frac{v^L}{|v^L|} + \frac{v^L \otimes v^L}{|v^L|^2} \langle \sigma \otimes \sigma : \nabla_{v^L}^2 f^L \rangle \right) \right\}, \end{aligned}$$

where

$$(3.3) \quad \langle f \rangle = \int_{\mathbb{S}^1} f(\sigma) d\sigma.$$

When  $v^L = 0$ , we have

$$Q_0^{LH}(0) = 0, \quad Q_1^{LH}(0) = 2\pi B^{LH} n^H u^H \cdot \nabla_{v^L} f^L(0), \quad Q_2^{LH}(0) = 4\pi B^{LH} n^H f^L(0).$$

In addition, the heavy-light collision operators are given by

$$(3.4) \quad \begin{aligned} Q_0^{HL}(v^H) &= -2\pi B^{HL} \nabla_{v^H} f^H \cdot n^L u^L, \\ Q_1^{HL}(v^H) &= 2\pi B^{HL} (v^H \cdot \nabla_{v^H} f^H n^L + 2f^H n^L) \\ &\quad + \pi B^{HL} \Delta_{v^H} f^H \left( \frac{1}{2} n^L |u^L|^2 + n^L T^L \right) \\ &\quad + \pi B^{HL} \nabla_{v^H}^2 f^H : \int_{\mathbb{R}^2} v^L \otimes v^L f^L dv^L. \end{aligned}$$

In the above formulae, the double dot product  $\mathbf{A} : \mathbf{B}$  is defined as

$$\mathbf{A} : \mathbf{B} = \sum_{i=1}^n \sum_{j=1}^n A_{ij} B_{ij}$$

for second-order tensors  $\mathbf{A}$  and  $\mathbf{B}$ , here the tensor product  $\mathbf{u} \otimes \mathbf{v}$  is defined as  $(\mathbf{u} \otimes \mathbf{v})_{ij} = u_i v_j$  for vectors  $\mathbf{u}$  and  $\mathbf{v}$ .

**3.2. Evaluation of collision operators in AE method.** In this subsection, we will carefully study how to numerically implement the collision operators (3.2) and (3.4) appeared in the AE method. We consider two-dimensional velocity variable with computational domain  $[-L_v, L_v]^2$ . Assume that  $f^L(v)$  and  $f^H(v)$  are periodic in  $v$ , and the length  $L_v$  is chosen within which  $f^L(v)$  and  $f^H(v)$  are compactly supported. The supports and  $L_v$  satisfy the de-aliasing condition in [27].

From (3.4), we notice that  $Q_0^{HL}$ ,  $Q_1^{HL}$  only involve simple operations including differentiation and integration, which can be computed by central difference and trapezoidal rule. The main challenge of computing the light-heavy collision operators (3.2) lies in the evaluation of angular integration, given  $f^L(v)$  defined on the Cartesian grid. Our main idea is to first interpolate the values of  $f^L(v)$  on the Cartesian grid into values  $f_{\text{pol}}^L(r, \sigma)$  defined on a polar grid, then evaluate the light-heavy collision operators in polar coordinates, finally interpolate the above values of collision operators back onto the Cartesian grid.

**3.2.1. Polar grid and interpolation.** For a non-zero vector  $v$ , let  $v = r\sigma = r(\cos \theta, \sin \theta)$ , where  $r \in (0, |v|_{\text{max}}]$  and  $\theta \in [0, 2\pi)$ . The angle  $\theta$  is discretized periodically into  $N_\theta$  grid points:

$$0 = \theta_1 < \theta_2 < \dots < \theta_{N_\theta},$$

where  $\theta_i = (i-1)\frac{2\pi}{N_\theta}$  for  $i = 1, \dots, N_\theta$ . To avoid the origin, the radial component  $r$  is discretized into  $N_r$  grid points defined by

$$\frac{\Delta r}{2} = r_1 < r_2 < \dots < r_{N_r} = |v|_{\text{max}} - \frac{\Delta r}{2},$$

where  $r_{j+1} - r_j = \Delta r$  for  $j = 1, \dots, N_r - 1$ , and the mesh size is  $\Delta r = \frac{|v|_{\text{max}}}{N_r}$ . We let  $N_r = N_v/2$ ,  $N_\theta = N_v$  and show the layout of a Cartesian grid and a polar grid with  $N_v = 30$  in Figure 3.1. In our simulations, much finer grids are used. We give some remarks about this Cartesian-Polar grid design. To begin with, the

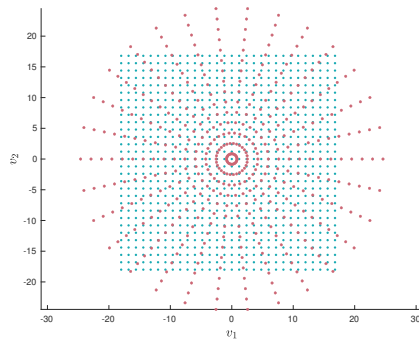


Fig. 3.1: Illustration of grid design with  $N_v = 30$

velocity domains covered by the two types of grids are different. In addition, the Cartesian grid is built on a uniform mesh, while the polar grid exhibit a clustering

phenomenon near the centered point and becomes sparser as the radius increases. As mentioned in [27], in fact  $S \approx 0.38L_v$ , with  $S$  being the support of distribution functions. This indicates that the supports of  $f^L$ ,  $f^H$  are concentrated near the centered point, thus the accuracy loss brought by the polar grid layout in the region far away is relatively negligible, and it is safe to set the values on those ‘‘suburb’’ points to be zero. Developing a more evenly distributed polar grid design that equally works well, together with a more rigorous error analysis is deferred to our future work. Practically, we simply use MATLAB’s `interp` function with `makima` interpolation method to efficiently compute the interpolation between functions defined on the Cartesian and polar grids, which can prevent overshoots and produce satisfactory results.

**3.2.2. Collision operators in polar coordinates.** To transform the light-heavy collision operators for  $f_{\text{pol}}^L$  to polar coordinates, we need to rewrite (3.2). By a change of variable  $v = r\sigma = r(\cos\theta, \sin\theta)$ ,  $r \neq 0$ , the derivatives in  $v^L$  on a function  $f$  are given by

$$\nabla_{v^L} f = \begin{pmatrix} \partial_{v_1^L} f \\ \partial_{v_2^L} f \end{pmatrix} = \begin{pmatrix} \cos\theta \partial_r f - \frac{1}{r} \sin\theta \partial_\theta f \\ \sin\theta \partial_r f + \frac{1}{r} \cos\theta \partial_\theta f \end{pmatrix}, \quad \nabla_{v^L}^2 f = \begin{pmatrix} \partial_{v_1^L v_1^L} f & \partial_{v_1^L v_2^L} f \\ \partial_{v_1^L v_2^L} f & \partial_{v_2^L v_2^L} f \end{pmatrix},$$

where

$$\begin{aligned} \partial_{v_1^L v_1^L} f &= \cos^2\theta \partial_{rr}^2 f - \frac{2}{r} \cos\theta \sin\theta \partial_{r\theta}^2 f + \frac{\sin^2\theta}{r^2} \partial_{\theta\theta}^2 f \\ &\quad + 2 \frac{\cos\theta \sin\theta}{r^2} \partial_\theta f + \frac{\sin^2\theta}{r} \partial_r f, \\ \partial_{v_2^L v_2^L} f &= \sin^2\theta \partial_{rr}^2 f + \frac{2}{r} \cos\theta \sin\theta \partial_{r\theta}^2 f + \frac{\cos^2\theta}{r^2} \partial_{\theta\theta}^2 f \\ &\quad - 2 \frac{\cos\theta \sin\theta}{r^2} \partial_\theta f + \frac{\cos^2\theta}{r} \partial_r f, \\ \partial_{v_1^L v_2^L} f &= \cos\theta \sin\theta \partial_{rr}^2 f + \frac{\cos^2\theta - \sin^2\theta}{r} \partial_{r\theta}^2 f - \frac{\sin\theta \cos\theta}{r^2} \partial_{\theta\theta}^2 f \\ &\quad + \frac{\sin^2\theta - \cos^2\theta}{r^2} \partial_\theta f - \frac{\sin\theta \cos\theta}{r} \partial_r f. \end{aligned}$$

Based on the above expressions, one can apply integration by parts to eliminate derivatives in  $\theta$ , then get

$$\begin{aligned} (3.5) \quad Q_0^{LH}(v^L) &= B^{LH} n^H [\langle f^L \rangle - 2\pi f^L], \\ Q_1^{LH}(v^L) &= B^{LH} n^H \left\{ u_1^H \left[ \langle \cos\theta \partial_r f^L \rangle + \frac{1}{r} \langle \cos\theta f^L \rangle - \cos\theta \langle \partial_r f^L \rangle \right] \right. \\ &\quad \left. + u_2^H \left[ \langle \sin\theta \partial_r f^L \rangle - \frac{1}{r} \langle \sin\theta f^L \rangle - \sin\theta \langle \partial_r f^L \rangle \right] \right\}, \\ Q_2^{LH}(v^L) &= B^{LH} \{I_1 + I_2 + I_3 + I_4 + I_5\}, \end{aligned}$$

where  $\langle \cdot \rangle$  denotes the angular integration

$$\langle f \rangle := \int_{\mathbb{S}^1} f(r\cos\theta, r\sin\theta) d\theta.$$

With the following definitions

$$\begin{aligned} A_1 &= \langle \partial_{rr} f^L \rangle - \frac{1}{r} \langle \partial_r f^L \rangle, & A_2 &= \frac{1}{r} \langle \partial_r f^L \rangle, & A_5 &= \langle \partial_r f^L \rangle, \\ A_3 &= \partial_{rr} f^L + \frac{3}{r} \partial_r f^L + \frac{2}{r^2} f^L, & A_4 &= \partial_{rr} f^L + \frac{1}{r} \partial_r f^L - \frac{1}{r^2} f^L, \end{aligned}$$

the components  $I_1$  through  $I_5$  are given by

$$\begin{aligned} I_1 &= 2n^H \langle f^L \rangle - \cos \theta \langle \cos \theta f^L \rangle - \sin \theta \langle \sin \theta f^L \rangle, \\ I_2 &= n^H r A_5 + \left( \frac{1}{2} n^H |u^H|^2 + n^H T^H \right) A_2, \\ I_3 &= -n^H r \left( \cos \theta \langle \cos \theta \partial_r f^L \rangle + \sin \theta \langle \sin \theta \partial_r f^L \rangle \right), \\ I_4 &= \frac{1}{2} \int (v_1^H)^2 f^H dv^H \left[ \cos^2 \theta A_1 + \langle \cos^2 \theta \partial_{rr} f^L \rangle \right. \\ &\quad \left. + \frac{1}{r} \langle (2 \cos^2 \theta - \sin^2 \theta) \partial_r f^L \rangle - 2 \cos \theta \langle \cos \theta A_4 \rangle \right], \\ I_5 &= \int v_1^H v_2^H f^H dv^H \left[ \cos \theta \sin \theta A_1 + \langle \cos \theta \sin \theta A_3 \rangle - \cos \theta \langle \cos \theta A_4 \rangle \right. \\ &\quad \left. - \sin \theta \langle \sin \theta A_4 \rangle \right] + \frac{1}{2} \int (v_2^H)^2 f^H dv^H \left[ \sin^2 \theta A_1 + \langle \sin^2 \theta \partial_{rr} f^L \rangle \right. \\ &\quad \left. + \frac{1}{r} \langle (2 \sin^2 \theta - \cos^2 \theta) \partial_r f^L \rangle - 2 \sin \theta \langle \sin \theta A_4 \rangle \right], \end{aligned}$$

Note that the numerical computations are reduced to integrals in  $\theta$  and derivatives in  $r$ . Thanks to the polar-grid design, for the asymptotic operators shown in (3.5), we can efficiently evaluate the angular integration by using the trapezoidal rule; while differentiation in  $r$  can be computed by the standard central difference method.

**3.3. Computational efficiency.** We refer to the modified spectral method (compared to the traditional fast spectral method in [27]) as the **SP** method, and our asymptotic-expansion (AE) studied in Section 3.1 as the **AE** method. The details of **SP** method are shown in Appendix A. In this part, we compare the **AE** and the **SP** method in terms of computational efficiency. The **SP** method, although built upon a fast spectral approach, can only achieve a computational complexity of  $\mathcal{O}(N_v^{2d_v})$ . This is due to the direct evaluation of Fourier (A.5) and their inverse transforms (A.6); additionally it is worsened by the small parameter  $\varepsilon$  especially when  $\varepsilon \ll 1$ .

**PROPOSITION 3.1.** *Our **SP** method has a time complexity of  $\mathcal{O}((N_v(\varepsilon))^{2d_v})$ , with  $N_v(\varepsilon) \propto 1/\varepsilon$ .*

*Proof.* In the **SP** method, we assume  $\text{Supp}(\tilde{f}^H) \subset \mathcal{B}_{\varepsilon S}$ . Here,  $\text{Supp}(\tilde{f}^H)$  denotes the support of  $\tilde{f}^H$ , and  $\mathcal{B}_S$  is the ball in  $\mathbb{R}^{d_v}$  centered at the origin with radius  $S$ . By the Heisenberg's inequality [14], one has

$$|\text{Supp}(\tilde{f}^H)| \cdot |\text{Supp}(\hat{f}_m^H)| \gtrsim 1,$$

where  $|\cdot|$  denotes the measure of a set,  $\tilde{f}^H$  and  $\hat{f}_m^H$  are defined in (A.5). Therefore,

$$|\text{Supp}(\hat{f}_m^H)| \approx 1/\varepsilon.$$

To accurately capture this change in computational domain from  $\tilde{f}^H$  to  $\hat{f}_m^H$ , for the velocity discretization  $N_v(\varepsilon) \propto 1/\varepsilon$  points are needed.  $\square$

On the other hand, our **AE** method provides a computationally more feasible approach by reducing the nonlinearity of the original collision operators to purely quadratic terms that only involve derivatives and integrals on a polar grid. The computational complexity of level  $\mathcal{O}(N_v^{d_v})$  is attained. More importantly, thanks to the asymptotic analysis, the computational complexity of **AE** method is independent of  $\varepsilon$ , making it advantageous to efficiently compute the inter-particle collision operators especially in regimes with widely disparate mass mixture (i.e.,  $\varepsilon \ll 1$ ), where the **SP** method fails to achieve.

**4. Asymptotic-preserving (AP) method.** In this section, we introduce the time discretization of (2.3) and will show its asymptotic-preserving (AP) property. Our AP scheme is derived based on the BGK-penalization technique first proposed by Filbet and Jin [12], and inspired by the study in [17]. The discretized scheme reads:

$$(4.1) \quad \begin{aligned} \frac{f_L^{n+1} - f_L^n}{\Delta t} &= \frac{1}{\varepsilon^2} (Q^{LL}(f_L^n, f_L^n) + Q_{\text{AE}}^{LH}(f_L^n, f_H^n) - \beta_L^n(M_L^n - f_L^n)) \\ &\quad + \frac{1}{\varepsilon^2} \beta_L^{n+1}(M_L^{n+1} - f_L^{n+1}), \\ \frac{f_H^{n+1} - f_H^n}{\Delta t} &= \frac{1}{\varepsilon} (Q^{HH}(f_H^n, f_H^n) + Q_{\text{AE}}^{HL}(f_H^n, f_L^n) - \beta_H^n(M_H^n - f_H^n)) \\ &\quad + \frac{1}{\varepsilon} \beta_H^{n+1}(M_H^{n+1} - f_H^{n+1}), \end{aligned}$$

where  $n$  stands for the time step and the computational time  $t = n\Delta t$ . Here  $M_L^n$  and  $M_H^n$  are Maxwellians associated with  $f_L^n$  and  $f_H^n$ .

One of the advantages of the BGK-penalization approach lies in the possibility of directly obtaining  $M_L^{n+1}$  and  $M_H^{n+1}$ , rendering the implicit method (4.1) explicit. Inspired by the idea in [18], we make use of the macroscopic equations (2.8) and update  $M_L^{n+1}$  and  $M_H^{n+1}$  from the macroscopic system *simultaneously* at each time step. In particular, simply applying the forward Euler method on (2.8), one has

$$(4.2) \quad \begin{aligned} n_L^{n+1} &= n_L^n, & n_H^{n+1} &= n_H^n, \\ u_L^{n+1} &= u_L^n, & u_H^{n+1} &= u_H^n, \\ \frac{n_L^{n+1}T_L^{n+1} - n_L^nT_L^n}{\Delta t} &= -2\frac{\lambda(T_L^n)}{T_L^n}n_L^n n_H^n(T_L^n - T_H^n), \\ \frac{n_H^{n+1}T_H^{n+1} - n_H^nT_H^n}{\Delta t} &= -2\frac{\lambda(T_L^n)}{T_L^n}n_L^n n_H^n(T_H^n - T_L^n). \end{aligned}$$

Then the Maxwellians needed in (4.1) are obtained:

$$M_L^{n+1}(v) := \mathcal{M}_{n_L^{n+1}, u_L^{n+1}, T_L^{n+1}}(v), \quad M_H^{n+1}(v) := \mathcal{M}_{n_H^{n+1}, u_H^{n+1}, T_H^{n+1}}(v).$$

**The penalty parameter  $\beta$ .** In the BGK-penalization approach,  $\beta_L$  and  $\beta_H$  are positive constants chosen for stability, which was discussed in [12, 17, 36]. In the case of the Boltzmann operator  $Q$ , one typical choice of the parameter  $\beta$  is given by  $\beta > Q^-$ , in which the decomposition of the Boltzmann collision operator  $Q = Q^+ - fQ^-$

is made. The definition of  $Q^-$  is given by

$$(4.3) \quad Q^-(f, f) = \int_{\mathbb{R}^{d_v} \times \mathbb{S}^{d_v-1}} B(|v - v_1|, \sigma) f(v_1) \, d\sigma \, dv_1.$$

This approach guarantees the positivity of the numerical solutions [36]. Here, we adopt the same approach by choosing

$$(4.4) \quad \beta_L > Q^{LL,-} + Q_\varepsilon^{LH,-}, \quad \beta_H > Q^{HH,-} + Q_\varepsilon^{HL,-},$$

where  $Q^{LL,-}$ ,  $Q_\varepsilon^{LH,-}$ ,  $Q^{HH,-}$  and  $Q_\varepsilon^{HL,-}$  are defined similarly as (4.3).

**4.1. The AP property.** We prove the following theorem on the weak AP property [12] of the scheme (4.1)-(4.2)

**THEOREM 4.1.** *The numerical solutions  $f_L^n$  and  $f_H^n$  given by (4.1)-(4.2) satisfy the following property: If  $f_L^n - M_L^n = \mathcal{O}(\varepsilon)$  and  $f_H^n - M_H^n = \mathcal{O}(\varepsilon)$ , then  $f_L^{n+1} - M_L^{n+1} = \mathcal{O}(\varepsilon)$  and  $f_H^{n+1} - M_H^{n+1} = \mathcal{O}(\varepsilon)$ . In particular, as  $\varepsilon \rightarrow 0$ , the numerical scheme (4.1)-(4.2) automatically becomes a consistent discretization of the macroscopic limit equation (2.8), thus satisfies the AP property.*

*Proof.* An algebraic rearrangement of (4.1) gives

$$(4.5) \quad \begin{aligned} f_L^{n+1} &= \frac{\beta_L^{n+1} \Delta t}{\varepsilon^2 + \beta_L^{n+1} \Delta t} M_L^{n+1} + \frac{\varepsilon^2}{\varepsilon^2 + \beta_L^{n+1} \Delta t} f_L^n \\ &\quad + \frac{\Delta t}{\varepsilon^2 + \beta_L^{n+1} \Delta t} (Q^{LL}(f_L^n, f_L^n) + Q_{AE}^{LH}(f_L^n, f_H^n) - \beta_L^n (M_L^l - f_L^n)), \\ f_H^{n+1} &= \frac{\beta_H^{n+1} \Delta t}{\varepsilon + \beta_H^{n+1} \Delta t} M_H^{n+1} + \frac{\varepsilon}{\varepsilon + \beta_H^{n+1} \Delta t} f_H^n \\ &\quad + \frac{\Delta t}{\varepsilon + \beta_H^{n+1} \Delta t} (Q^{HH}(f_H^n, f_H^n) + Q_{AE}^{HL}(f_H^n, f_L^n) - \beta_H^n (M_H^l - f_H^n)). \end{aligned}$$

First, as  $\varepsilon \rightarrow 0$  in (4.5) the coefficients of  $M_L^{n+1}$  and  $M_H^{n+1}$ , namely  $\frac{\beta_L^{n+1} \Delta t}{\varepsilon^2 + \beta_L^{n+1} \Delta t}$  and  $\frac{\beta_H^{n+1} \Delta t}{\varepsilon + \beta_H^{n+1} \Delta t}$  both converge to 1. We only need to check that the other terms on the right-hand-side of equation (4.5) are of  $\mathcal{O}(\varepsilon)$ . By our assumption,  $f_L^n - M_L^n = \mathcal{O}(\varepsilon)$  and  $f_H^n - M_H^n = \mathcal{O}(\varepsilon)$ . Consequently, from the H-theorem (2.1) one has

$$Q^{LL}(f_L^n, f_L^n) = \mathcal{O}(\varepsilon), \quad Q^{HH}(f_H^n, f_H^n) = \mathcal{O}(\varepsilon).$$

In  $Q_{AE}^{LH}(f_L^n, f_H^n)$  and  $Q_{AE}^{HL}(f_H^n, f_L^n)$ , only the leading order terms appear to be  $\mathcal{O}(1)$ . Due to our assumption for  $f_L^n$ ,  $f_H^n$  and the property 1 in Theorem 2.3, we have

$$Q_0^{LH}(f_L^n, f_H^n) = \mathcal{O}(\varepsilon), \quad Q_0^{HL}(f_H^n, f_L^n) = \mathcal{O}(\varepsilon).$$

This finally leads to

$$f_L^{n+1} - M_L^{n+1} = \mathcal{O}(\varepsilon), \quad f_H^{n+1} - M_H^{n+1} = \mathcal{O}(\varepsilon).$$

Therefore, our numerical scheme (4.1)-(4.2) satisfies the AP property.  $\square$

**5. Numerical Examples.** In this section, we present several numerical examples to demonstrate the accuracy and efficiency of our numerical schemes. The mass ratio of the heavy species mass  $m_H$  and the light species  $m_L$  in our gas mixtures is related by

$$\varepsilon^2 = \frac{m_L}{m_H}.$$

We consider two-dimensional problem in velocity, with the computational domain  $v \in [-18, 18]^2$ . For simplicity, collision kernels are given as

$$B^{LL} = B^{HH} = \frac{1}{4\pi}, \quad B^{LH} = B^{HL} = \frac{1}{8\pi}.$$

The collision frequency in (2.8) becomes

$$(5.1) \quad \lambda(T^L) = 2\pi B^{HL} T^L.$$

Let the initial distributions be the double-peak Maxwellian defined by

$$(5.2) \quad f^L = \frac{n^L}{4\pi T^L} \left( e^{-\frac{|v+u_1^L|^2}{2T^L}} + e^{-\frac{|v+u_2^L|^2}{2T^L}} \right), \quad f^H = \frac{n^H}{4\pi T^H} \left( e^{-\frac{|v+u_1^H|^2}{2T^H}} + e^{-\frac{|v+u_2^H|^2}{2T^H}} \right),$$

where

$$n^L = n^H = 1, \quad T^L = 1, \quad T^H = 0.5, \\ u_1^L = (1.2, 0), \quad u_2^L = -(0.5, 0), \quad u_1^H = -(1.2, 0), \quad u_2^H = (0.5, 0).$$

All Numerical experiments were conducted on a high-performance GPU server with Dual Intel Xeon Gold 6230 CPUs, 1 TB RAM, and 8 NVIDIA Quadro RTX 8000 GPUs.

**5.1. Test I.** In this test, we solve the non-stiff time evolution problem (2.2) using (i) the **SP** method, and (ii) the **AE** method for the evaluation of the inter-particle operators  $Q_\varepsilon^{LH}$ ,  $Q_\varepsilon^{HL}$ . We study from the following aspects: convergence order, computational efficiency, and conservation of collision operators computed by the two approaches.

**Convergence order.** We first test the convergence of numerical solutions in the velocity space and across different mass disparity regimes. For the **AE** method, we study four cases of gas mixtures characterized by decreasing  $\varepsilon$  values of 0.5,  $1 \times 10^{-1}$ ,  $3 \times 10^{-2}$ , and  $1 \times 10^{-2}$ . The velocity discretization are chosen by  $N_v = 30, 60, 120, 240$ , and 480 in all scenarios. For the **SP** method, on the other hand, as  $\varepsilon$  decreases, one needs to use significantly larger  $N_v$  values, which makes it computationally demanding. The details of  $\varepsilon$  and  $N_v$  are summarized in Table 1. We set the final computational time to be  $t = 0.5$  for all the tests.

$\varepsilon$	$N_v$
0.1	50, 100, 200, 400, 800
0.2	50, 100, 200, 400, 800
0.5	20, 40, 80, 160, 320
1	10, 20, 40, 80, 160

Table 1: Parameter settings for the **SP** method.

In Figure 5.1 and Figure 5.2, we present the the relative  $L^2$  errors of the solutions:

$$e_{N_v}(f) = \frac{\|f_{N_v} - f_{N_v/2}\|_{L^2}}{\|f_{N_v}\|_{L^2}},$$

where  $f_{N_v}$  denotes the numerical solution computed on a velocity grid of size  $N_v \times N_v$ . The numerical scheme is  $k$ -th order if  $e_{N_v}(f) \leq \frac{C}{N_v^k}$  for  $N_v \gg 1$ . For the **SP** method, a loss in accuracy using the same  $N_v$  is observed as  $\varepsilon$  gets smaller. Indeed, as discussed in Proposition 3.1, our **SP** method requires a computational cost of  $\mathcal{O}(N_v^4)$  with  $N_v \propto 1/\varepsilon$ . In addition, we compare the results with the first- and second-order convergence in velocity variable, shown in dotted lines. Thanks to the spectral accuracy of the **SP** method, the convergence in  $v$  is expected to be much faster than the first- and second-order convergence lines, which is observed for various  $\varepsilon$ . To maintain the same level of accuracy when  $\varepsilon$  is smaller, a finer velocity mesh becomes necessary, which is consistent with our theoretical findings in Appendix A.

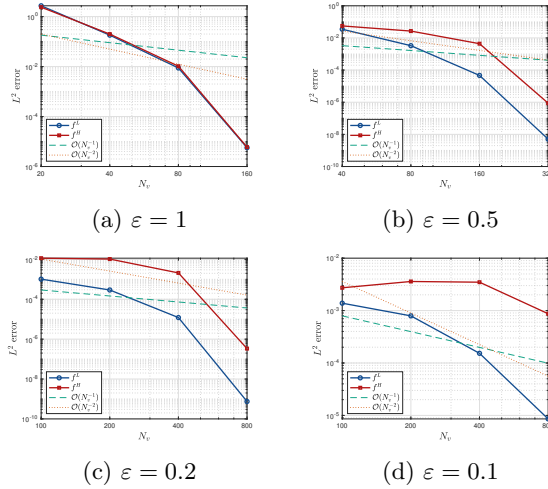
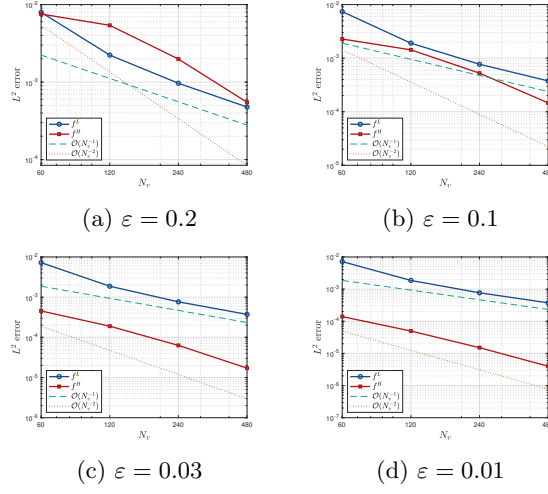


Fig. 5.1: Convergence error in  $L^2$  for the **SP** method.

On the contrary, from Figure 5.2 we observe that the **AE** method exhibits two distinguished properties. First, a slight deterioration of accuracy for the heavy species  $f^H$  as  $\varepsilon$  increases. This coincides with our expectations, since according to the nature of the asymptotic expansions (2.9), the asymptotic operators are unable to produce accurate results when  $\varepsilon$  is large. Second, the method demonstrates a *uniform* accuracy for the light species  $f^L$ , regardless of the values of  $\varepsilon$ . This behaviour of the numerical solutions benefits from the design of the **AE** method, where  $\varepsilon$  is decoupled from the collision operators. We find out that in regimes with smaller  $\varepsilon$ , the **AE** method exhibits first-order accuracy for the distribution  $f^L$  and second-order accuracy for the distribution  $f^H$ .

**Computational efficiency.** To investigate the efficiency of the **SP** and **AE** method, the computational time for both approaches are presented in Table 2 and Table 3.

The **SP** method suffers from a computational complexity of  $\mathcal{O}(N_v^4)$ , where  $N_v \propto 1/\varepsilon$ . Given that this method heavily relies on the Fourier transforms, GPU-parallelized

Fig. 5.2: Convergence of  $L^2$  errors for the **AE** method.

$\varepsilon \backslash N_v$	10	20	40	80	160
1	26.39	55.92	127.78	317.75	924.01

$\varepsilon \backslash N_v$	20	40	80	160	320
0.5	55.59	131.71	311.44	893.81	3229.12

$\varepsilon \backslash N_v$	50	100	200	400	800
0.2	174.03	452.95	1351.10	5695.96	33854.44
0.1	169.50	438.10	1298.88	5326.12	33221.87

Table 2: GPU Times (in seconds) for the **SP** method.

$\varepsilon \backslash N_v$	30	60	120	240	480
0.2	1.08	1.35	4.32	12.31	47.37
0.1	0.69	1.39	4.08	12.34	46.39
0.03	0.69	1.34	4.09	12.57	44.57
0.01	0.68	1.39	4.03	12.71	46.31

Table 3: CPU Times (in seconds) for the **AE** method.

implementations are particularly effective for accelerating computations ([22]). However, even by using the GPU, significant computational cost is observed from Table 2, especially for cases where  $\varepsilon = 0.1$  and  $\varepsilon = 0.2$ . This indicates that applying the spectral method to evaluate inter-particle collision operators in regimes with highly disparate masses ( $\varepsilon \ll 1$ ) seems computationally prohibitive, thus developing our **AE** method becomes a necessary and timely task.

The **AE** method, on the contrary, owns a much lower computational complexity

of  $\mathcal{O}(N_v^2)$  with  $N_v$  independent of  $\varepsilon$ . As shown in Table 3, even by using the standard CPU, the computational time remain consistently low in all  $\varepsilon$  regimes. We conclude that our **AE** method guarantees a *uniformly low* computational complexity across disparate mass regimes, rendering the method particularly accurate and efficient for gas mixture simulations in disparate mass regimes (when  $\varepsilon \ll 1$ ).

Regarding the computational efficiency in different mass disparity regimes, we summarize the following observations: the **SP** method achieves optimal performance for mixtures with nearly equal masses ( $\varepsilon \approx 1$ ), whereas becomes computationally infeasible in disparate mass regimes due to increasingly stringent requirements in velocity discretization that is  $\varepsilon$  dependent. The **AE** method, on the other hand, demonstrates a *uniformly cheap* computational cost and works consistently well in disparate mass regime where  $\varepsilon \ll 1$ . Figure 5.3 shows the regimes with different  $\varepsilon$  where either **AE** or **SP** approach is effective. We call the regime where  $\varepsilon$  is relatively small (but not too small) an “overlapping regime” where both methods work, and compare the numerical solutions obtained by these two methods in the next part.

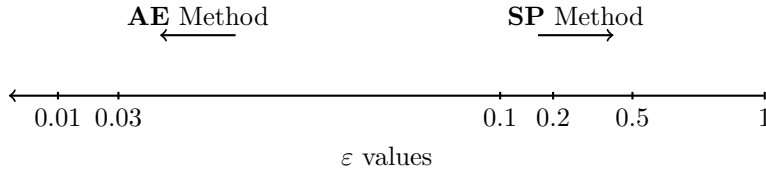
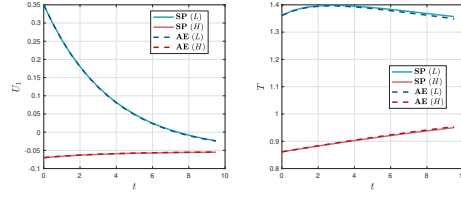
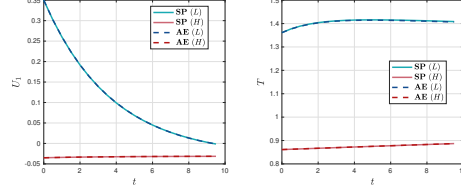


Fig. 5.3: Different  $\varepsilon$  regimes that show the effectiveness of two methods.

**Overlapping regime.** To ensure both methods are effective and accurate, we let  $\varepsilon = 0.2, 0.1$  in the so-called overlapping regime, and present in Figure 5.4 the time evolution of first direction of velocity vector ( $U_1$ ) and temperature ( $T$ ) solved by (2.2). The dashed lines represent the numerical solutions obtained using the **AE** method, while the solid lines stand for those computed with the **SP** method. For the **AE** method, a velocity grid size of  $N_v = 480$  is used, whereas the **SP** method uses  $N_v = 800$ . Both methods are implemented with a time step of  $\Delta t = 0.5$ .

**Conservation properties.** We conclude by validating the conservation properties outlined in Theorem 2.3. The following quantities

$$\begin{aligned}
\mathcal{M}_\varepsilon^{LH} &= \int_{\mathbb{R}^{d_v}} Q_\varepsilon^{LH} dv, & \mathcal{M}_\varepsilon^{HL} &= \int_{\mathbb{R}^{d_v}} Q_\varepsilon^{HL} dv, \\
\mathcal{U}_\varepsilon &= \int_{\mathbb{R}^{d_v}} Q_\varepsilon^{LH} v dv + Q_\varepsilon^{HL} v dv, & \mathcal{E}_\varepsilon &= \int_{\mathbb{R}^{d_v}} Q_\varepsilon^{LH} |v|^2 dv + \varepsilon Q_\varepsilon^{HL} |v|^2 dv, \\
\mathcal{M}_0^{LH} &= \int_{\mathbb{R}^{d_v}} Q_0^{LH} dv, & \mathcal{M}_1^{LH} &= \int_{\mathbb{R}^{d_v}} Q_1^{LH} dv, & \mathcal{M}_2^{LH} &= \int_{\mathbb{R}^{d_v}} Q_2^{LH} dv, \\
\mathcal{M}_0^{HL} &= \int_{\mathbb{R}^{d_v}} Q_0^{HL} dv, & \mathcal{M}_1^{HL} &= \int_{\mathbb{R}^{d_v}} Q_1^{HL} dv, \\
\mathcal{U}_0 &= \int_{\mathbb{R}^{d_v}} Q_0^{LH} v dv + Q_0^{HL} v dv, & \mathcal{U}_1 &= \int_{\mathbb{R}^{d_v}} Q_1^{LH} v dv + Q_1^{HL} v dv, \\
\mathcal{E}_0 &= \int_{\mathbb{R}^{d_v}} Q_0^{LH} |v|^2 dv, & \mathcal{E}_1 &= \int_{\mathbb{R}^{d_v}} Q_1^{LH} |v|^2 dv + Q_0^{HL} |v|^2 dv, \\
\mathcal{E}_2 &= \int_{\mathbb{R}^{d_v}} Q_2^{LH} |v|^2 dv + Q_1^{HL} |v|^2 dv,
\end{aligned}$$

(a)  $\varepsilon = 0.2$ (b)  $\varepsilon = 0.1$ Fig. 5.4: Test I. Evolution of the first direction of velocities ( $U_1$ ) and temperatures ( $T$ ).

were computed at time  $t = 0.5$  for the case  $\varepsilon = 0.1$ , where the collision operators with subscript ‘ $\varepsilon$ ’ are calculated using the **SP** method, while the others are obtained using the **AE** method. As shown in Table 4, these quantities are well preserved, cross-validating the accuracy of both methods. Furthermore, the conservation properties of the collision operators ensure that the solutions exhibit the correct macroscopic behavior.

$\mathcal{C}$	$N_v$		
	100	200	400
$\mathcal{M}_\varepsilon^{LH}$	-4.3e-6	1.1e-6	5.5e-9
$\mathcal{M}_\varepsilon^{HL}$	7.3e-3	-2.8e-3	-1.1e-4
$\mathcal{U}_\varepsilon$	2.8e-2	-4.8e-3	6.0e-3
$\mathcal{E}_\varepsilon$	1.5e-1	-7.6e-2	-3.2e-3

$\mathcal{C}$	$N_v$		
	80	160	320
$\mathcal{M}_0^{LH}$	-4.9e-3	-2.4e-3	-1.2e-3
$\mathcal{M}_1^{LH}$	-3.8e-4	-1.0e-4	-2.4e-5
$\mathcal{M}_2^{LH}$	-1.2e-2	-3.1e-3	-6.8e-4
$\mathcal{M}_0^{HL}$	-2.1e-17	4.8e-18	1.2e-18
$\mathcal{M}_1^{HL}$	-8.5e-15	-9.4e-17	7.1e-17
$\mathcal{U}_0$	-5.6e-4	-2.0e-4	-9.0e-5
$\mathcal{U}_1$	-3.0e-3	-2.2e-4	1.6e-4
$\mathcal{E}_0$	-1.8e-2	-8.9e-3	-4.5e-3
$\mathcal{E}_1$	-3.4e-3	-2.2e-3	-1.2e-3
$\mathcal{E}_2$	-3.8e-1	-9.4e-2	-2.1e-2

Table 4: Conserved quantities for  $\varepsilon = 0.1$  using **SP** (left) and **AE** (right) methods.

**5.2. Test II.** In this test, we focus on the stiff problem (2.3) in the disparate mass regime ( $\varepsilon \ll 1$ ). The **AE** method is employed to evaluate the inter-particle collision operators, and AP scheme (4.1)-(4.2) is used for temporal discretization, which tackles the stiffness of the system while capturing its macroscopic behaviour.

The goal of this test is to demonstrate the ability of our scheme to solve the Boltzmann equation for gas mixtures with disparate masses, while ensuring consis-

tency with the macroscopic equations (2.8). We consider the cases  $\varepsilon = 0.1$ ,  $\varepsilon = 0.03$  and  $\varepsilon = 0.01$ , corresponding to gas mixtures with mass ratios ranging from  $10^2$  to  $10^4$ .

**Epochal relaxation.** Figure 5.5 shows the time evolution of the first direction of velocity vector ( $U_1$ ) and temperature ( $T$ ). Dashed lines represent the solutions obtained by the asymptotic-preserving (AP) scheme (4.1), whereas solid lines stand for the numerical solutions of the macroscopic system (2.8), which are discretized by using the first-order forward Euler scheme (4.2). For the AP scheme, we let  $N_v = 320$  and  $\Delta t = 0.015$ ; while  $\Delta t = 10^{-4}$  is used in the Euler method. Note that both velocities  $u^L$  and  $u^H$  in the macroscopic equations remain constant over time in our test, thus we omit drawing them in the plots on the top.

Figure 5.5 reveals several phenomena: (i) the rate of relaxation to the steady state for the velocity variable of light species is much larger than that of the heavy species; (ii) As  $\varepsilon$  decreases, the decay of velocity occurs faster—noted by a steeper slope in the plots on the top—with the equilibrium state getting closer to zero when  $T$  is large enough; (iii) Regarding the temperature variable, by comparing the AP scheme for the mixture model with the Euler method for the macroscopic equations, we observe that both solutions converge to the same steady state when time is sufficiently large and relaxation process ends. This meets our expectations and is exactly the AP property of our numerical scheme (4.1)-(4.2) that we desire.

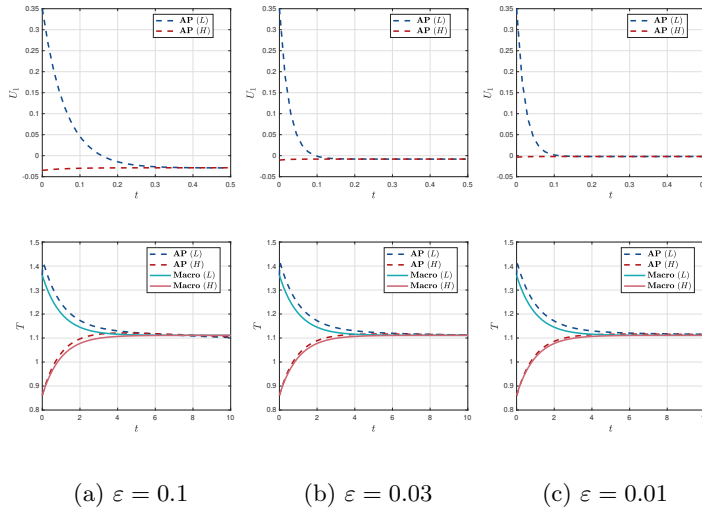


Fig. 5.5: Test II. Evolution of the first direction of the velocities ( $U_1$ ) and temperatures ( $T$ ).

**The AP property.** To validate the AP property of our proposed scheme, Figure 5.6 shows the time evolution of  $\|f^L - M^L\|_{L^2}$  and  $\|f^H - M^H\|_{L^2}$  across different values of  $\varepsilon$ . We thereby have the following main observations: (i) Even in the more general case when the initial distributions (5.2) are away from the Maxwellians, the AP property in Theorem 4.1 remains true, in particular,  $\|f^L - M^L\| = \mathcal{O}(\varepsilon)$  and  $\|f^H - M^H\| = \mathcal{O}(\varepsilon)$ ; (ii) Comparing the two plots in Figure 5.6, one can see that the relaxation process

of the heavy species is slightly slower than that of the light species; (iii) For both light and heavy species, the smaller the  $\varepsilon$  is, the smaller the errors of  $\|f^L - M^L\|$  and  $\|f^H - M^H\|$  are when saturated, at the level of roughly  $\mathcal{O}(\varepsilon^2)$ .

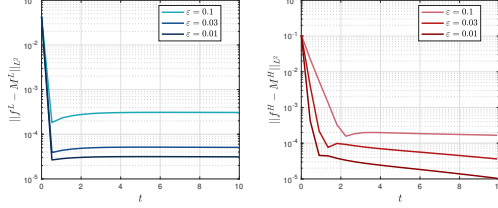


Fig. 5.6: Test II. Time evolution of  $\|f^L - M^L\|_{L^2}$  and  $\|f^H - M^H\|_{L^2}$  for different  $\varepsilon$ .

**6. Conclusion.** In this study, we developed asymptotic-preserving schemes for the Boltzmann mixture model with disparate mass. Our approach circumvents the prohibitive computational costs of traditional spectral methods by conducting asymptotic expansions in order to approximate the collision operators, especially when the mass disparity is huge. We consider the space-homogeneous problem and consider the longest time scale among the three time scales. Our AP scheme can accurately capture the epochal relaxation phenomenon, without resolving the small scaling parameter characterized by the square-root of mass ratio. Several numerical examples have demonstrated the effectiveness and efficiency of our AP scheme across a wide range of mass ratios. This work provides a solid foundation for future studies on the more complex disparate mass system, including the space-inhomogeneous problem.

## Appendices

**A. Scaled spectral method.** In this section, we provide a brief overview of the spectral method for evaluating the scaled operators  $Q_\varepsilon^{LH}$  and  $Q_\varepsilon^{HL}$ . This approach is an adaptation of the fast spectral method developed by [21] (hereafter referred to as the Jaiswal-Alexeenko-Hu method), with necessary modifications to account for the effects of scaling.

To address the scaling issue, our approach is to first reverse the scaling of the solutions, allowing the use of the Jaiswal-Alexeenko-Hu method to evaluate the collision operators. Once the collision operators have been computed, we then reapply the scaling to the resulting solutions.

**A.1. Re-scaling of operators.** We first perform a set of variable changes

$$(A.1) \quad \tilde{v}^H = \varepsilon v^H, \quad f^H(v^H) = \varepsilon^{d_v} \tilde{f}^H(\tilde{v}^H), \quad Q_\varepsilon^{HL}(f^H, f^L)(v^H) = \varepsilon^{d_v} \tilde{Q}_\varepsilon^{HL}(\tilde{v}^H),$$

to get

$$(A.2) \quad Q_\varepsilon^{LH}(v^L) = \sqrt{1 + \varepsilon^2} \int_{\mathbb{R}^{d_v} \times \mathbb{S}^{d_v-1}} B^{LH} \left( \frac{|g^{LH}|}{\sqrt{1 + \varepsilon^2}}, \sigma \cdot \hat{g}^{LH} \right) \\ \times \left[ f^L(v'^L) \tilde{f}^H(\tilde{v}'^H) - f^L(v^L) \tilde{f}^H(\tilde{v}^H) \right] d\sigma dg^{LH},$$

with collision rules

$$\begin{cases} v'^L = v^L - \frac{1}{1+\varepsilon^2}g^{LH} + \frac{1}{1+\varepsilon^2}|g^{LH}|\sigma, \\ \tilde{v}'^H = v^L - \frac{1}{1+\varepsilon^2}g^{LH} - \frac{\varepsilon^2}{1+\varepsilon^2}|g^{LH}|\sigma, \end{cases}$$

and

$$(A.3) \quad \begin{aligned} \tilde{Q}_\varepsilon^{HL}(\tilde{v}^H) &= \frac{\sqrt{1+\varepsilon^2}}{\varepsilon} \int_{\mathbb{R}^{d_v} \times \mathbb{S}^{d_v-1}} B^{HL} \left( \frac{|g^{HL}|}{\sqrt{1+\varepsilon^2}}, \sigma \cdot \hat{g}^{HL} \right) \\ &\quad \times \left[ \tilde{f}^H(\tilde{v}'^H) f^L(v'^L) - \tilde{f}^H(\tilde{v}^H) f^L(v^L) \right] d\sigma dg^{HL}, \end{aligned}$$

with collision rules

$$\begin{cases} \tilde{v}'^H = \tilde{v}^H - \frac{\varepsilon^2}{1+\varepsilon^2}g^{HL} + \frac{\varepsilon^2}{1+\varepsilon^2}|g^{HL}|\sigma, \\ v'^L = \tilde{v}^H - \frac{\varepsilon^2}{1+\varepsilon^2}g^{HL} - \frac{1}{1+\varepsilon^2}|g^{HL}|\sigma. \end{cases}$$

The integrations in  $\tilde{v}^H$  and  $v^L$  are transformed into integrations in  $g^{LH} = v^L - \tilde{v}^H$  and  $g^{HL} = \tilde{v}^H - v^L$ , respectively.

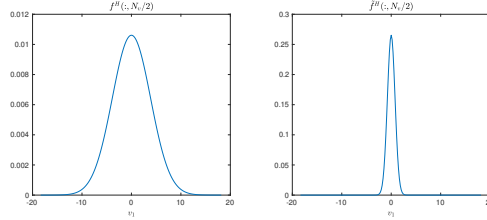


Fig. A.1: The distribution function before (left) and after (right) re-scaling.

**A.2. Jaiswal-Alexeenko-Hu method.** With the new velocity variables  $v^L$  and  $\tilde{v}^H$  on the same scale, we now apply the Jaiswal-Alexeenko-Hu method to solve (A.2) and (A.3).

### Step 1

Determine the velocity domain  $\mathcal{D}_L = [-L, L]^2$  and periodize  $f^L$  and  $\tilde{f}^H$  to  $\mathbb{R}^2$ . Following a similar analysis as in [21, 29], a support analysis can be conducted to give:

PROPOSITION A.1. *Let  $\text{Supp}(f^L(v^L)) \subset \mathcal{B}_S$ ,  $\text{Supp}(f^H(v^H)) \subset \mathcal{B}_S$ , then*

1.  $\text{Supp}(Q_\varepsilon^{LH}(v^L)) \subset \mathcal{B}_{\sqrt{2}S}$ ,  $\text{Supp}(\tilde{Q}_\varepsilon^{HL}(\tilde{v}^H)) \subset \mathcal{B}_{\varepsilon\sqrt{2}S}$ ,
2. *The integral in  $g^{LH}$  and  $g^{HL}$  can be truncated to a ball  $\mathcal{B}_R$  with  $R = (1+\varepsilon)S$ ,*
3. *De-aliasing condition:*

$$2L \geq (\sqrt{2} + 2 + 2\varepsilon)S + S.$$

### Step 2

Approximate the distribution functions by truncated Fourier series

$$f_{N_v}^L(v^L) = \sum_{l=-\frac{N_v}{2}}^{\frac{N_v}{2}-1} \hat{f}_l^L e^{i\frac{\pi}{L}v^L \cdot l}, \quad \tilde{f}_{N_v}^H(\tilde{v}^H) = \sum_{l=-\frac{N_v}{2}}^{\frac{N_v}{2}-1} \hat{f}_l^H e^{i\frac{\pi}{L}\tilde{v}^H \cdot l}$$

and substitute into (A.2). By performing the Galerkin projection to the same Fourier space

$$\hat{Q}_{\varepsilon,k}^{LH} = \frac{1}{(2L)^{d_v}} \sum_{\substack{l,m=-\frac{N_v}{2} \\ l+m=k}}^{\frac{N_v}{2}-1} G_\varepsilon^{LH}(l,m) \hat{f}_l^L \hat{f}_m^H, \quad k \in \{-\frac{N_v}{2}, \dots, \frac{N_v}{2} - 1\}.$$

The kernel modes are given by  $G_\varepsilon^{LH}(l,m) = G_\varepsilon^{LH,+}(l,m) - G_\varepsilon^{LH,-}(m)$ , with

$$G_\varepsilon^{LH,+}(l,m) = \sqrt{1+\varepsilon^2} \int_{\mathcal{B}_R \times \mathbb{S}^{d_v-1}} B^{LH} e^{-\frac{i\pi}{L} \frac{(l+m) \cdot g^{LH}}{1+\varepsilon^2} + \frac{i\pi}{L} \frac{|g^{LH}| \sigma \cdot (l-\varepsilon^2 m)}{1+\varepsilon^2}} d\sigma dg^{LH},$$

$$G_\varepsilon^{LH,-}(m) = \sqrt{1+\varepsilon^2} \int_{\mathcal{B}_R \times \mathbb{S}^{d_v-1}} B^{LH} e^{-\frac{i\pi}{L} m \cdot g^{LH}} d\sigma dg^{LH}.$$

The integration in  $g^{LH}$  is dealt with in spherical coordinates,

$$(A.4) \quad G_\varepsilon^{LH,+}(l,m) = \sqrt{1+\varepsilon^2} \int_0^R \int_{\mathbb{S}^{d_v-1}} F^{LH}(l+m, \rho, \sigma) e^{\frac{i\pi}{L} \rho \left[ \frac{l \cdot \sigma}{1+\varepsilon^2} - \frac{\varepsilon^2 m \cdot \sigma}{1+\varepsilon^2} \right]} d\sigma d\rho,$$

$$G_\varepsilon^{LH,-}(m) = \sqrt{1+\varepsilon^2} \int_0^R \int_{\mathbb{S}^{d_v-1}} \int_{\mathbb{S}^{d_v-1}} B^{LH} e^{-\frac{i\pi}{L} \rho m \hat{g}^{LH}} d\sigma d\hat{g}^{LH} d\rho,$$

where  $\rho = |g^{LH}|$ ,  $\hat{g}^{LH} = \frac{g^{LH}}{|g^{LH}|}$ , and

$$F^{LH}(l+m, \rho, \sigma) = \rho^{d_v-1} \int_{\mathbb{S}^{d_v-1}} B^{LH} e^{-\frac{i\pi}{L} \rho \frac{(l+m) \cdot \hat{g}^{LH}}{1+\varepsilon^2}} d\hat{g}^{LH}.$$

The idea of [21] is to precompute  $F^{LH}(l+m, \rho, \sigma)$  and  $G_\varepsilon^{LH,-}(m)$  up to a high accuracy, and approximate (A.4) *on the fly* using a quadrature rule.

In the case where  $d_v = 2$  and  $B^{LH}$ ,  $B^{HL}$  are constants,

$$G_\varepsilon^{LH,+}(l,m) \approx \sqrt{1+\varepsilon^2} \sum_{\rho,\sigma} w_\rho w_\sigma F^{LH}(l+m, \rho, \sigma) e^{\frac{i\pi}{L} \rho \left[ \frac{l \cdot \sigma}{1+\varepsilon^2} - \frac{\varepsilon^2 m \cdot \sigma}{1+\varepsilon^2} \right]}$$

$$= \sqrt{1+\varepsilon^2} B^{LH} \sum_{\rho,\theta} w_\rho w_\theta \rho e^{\frac{i\pi}{L} \rho \frac{|l \cos \theta - \varepsilon^2 m| \cos \theta}{1+\varepsilon^2}} \int_{\mathbb{S}^1} e^{-\frac{i\pi}{L} \rho \frac{(l+m) \cdot \hat{g}^{LH}}{1+\varepsilon^2}} d\hat{g}^{LH}.$$

For the radial direction, the Gauss-Legendre quadrature rule is used with  $N_\rho = \mathcal{O}(N_v)$  point. For the angular direction, rectangular rule is used. The integral in  $\hat{g}^{LH}$  can be directly evaluated using Bessel functions. In particular,

$$\int_{\mathbb{S}^1} e^{-\frac{i\pi}{L} \rho \frac{(l+m) \cdot \hat{g}^{LH}}{1+\varepsilon^2}} d\hat{g}^{LH} = \int_0^{2\pi} e^{-\frac{i\pi}{L} \rho \frac{|l+m| \cos \theta}{1+\varepsilon^2}} d\theta$$

$$= 2 \int_0^\pi \cos \left( \frac{\pi}{L} \rho \frac{|l+m| \cos \theta}{1+\varepsilon^2} \right) d\theta = 2\pi \mathcal{J}_0 \left( \frac{\pi}{L} \rho \frac{|l+m|}{1+\varepsilon^2} \right),$$

where  $\mathcal{J}_0(r) = \frac{1}{\pi} \int_0^\pi \cos(r \cos \theta) d\theta$ . Similarly,  $G_\varepsilon^{LH,-}(m)$  can be evaluated analytically as

$$\begin{aligned} G_\varepsilon^{LH,-}(m) &= \sqrt{1+\varepsilon^2} B^{LH} \int_0^R \rho \int_{\mathbb{S}^1} \int_{\mathbb{S}^1} e^{-\frac{i\pi}{L} \rho m \hat{g}^{LH}} d\sigma d\hat{g}^{LH} d\rho \\ &= 4\pi^2 R^2 B^{LH} \sqrt{1+\varepsilon^2} \int_0^1 s \mathcal{J}_0\left(\frac{R\pi}{L} |m| s\right) ds \\ &= \begin{cases} 4\pi^2 R^2 B^{LH} \sqrt{1+\varepsilon^2} \mathcal{J}_1\left(\frac{R\pi}{L} |m|\right) / \frac{R\pi}{L} |m|, & m \neq 0 \\ 2\pi^2 R^2 B^{LH} \sqrt{1+\varepsilon^2}, & m = 0. \end{cases} \end{aligned}$$

In summary, the computation of  $\hat{Q}_{\varepsilon,k}^{LH} = \hat{Q}_{\varepsilon,k}^{LH,+} - \hat{Q}_{\varepsilon,k}^{LH,-}$  can be carried out as follows

$$\begin{aligned} \hat{Q}_{\varepsilon,k}^{LH,+} &= 2\pi B^{LH} \sqrt{1+\varepsilon^2} \sum_{\rho,\theta} \sum_{l+m=k} w_\rho w_\theta \rho \mathcal{J}_0\left(\frac{\pi}{L} \rho \frac{|k|}{1+\varepsilon^2}\right) \hat{f}_l^L \hat{f}_m^H e^{i\frac{\pi}{L} \rho \frac{|l| \cos \theta - \varepsilon^2 |m| \cos \theta}{1+\varepsilon^2}}, \\ \hat{Q}_{\varepsilon,k}^{LH,-} &= \sum_{l+m=k}^{\frac{N_v}{2}-1} \hat{f}_l^L \left[ G_\varepsilon^{LH,-}(m) \hat{f}_m^H \right]. \end{aligned}$$

Following the same procedure, the computation of  $\hat{Q}_{\varepsilon,k}^{HL} = \hat{Q}_{\varepsilon,k}^{HL,+} - \hat{Q}_{\varepsilon,k}^{HL,-}$  is given by

$$\begin{aligned} \hat{Q}_{\varepsilon,k}^{HL,+} &= 2\pi B^{HL} \frac{\sqrt{1+\varepsilon^2}}{\varepsilon} \sum_{\rho,\theta} \sum_{l+m=k} \rho \mathcal{J}_0\left(\frac{\pi}{L} \rho \frac{\varepsilon^2 |k|}{1+\varepsilon^2}\right) \hat{f}_l^H \hat{f}_m^L e^{i\frac{\pi}{L} \rho \frac{\varepsilon^2 |l| \cos \theta - |m| \cos \theta}{1+\varepsilon^2}}, \\ \hat{Q}_{\varepsilon,k}^{HL,-} &= \sum_{l+m=k}^{\frac{N_v}{2}-1} \hat{f}_l^H \left[ G_\varepsilon^{HL,-}(m) \hat{f}_m^L \right], \end{aligned}$$

with

$$\begin{aligned} G_\varepsilon^{HL,-}(m) &= 4\pi^2 R^2 B^{HL} \frac{\sqrt{1+\varepsilon^2}}{\varepsilon} \int_0^1 s \mathcal{J}_0\left(\frac{R\pi}{L} |m| s\right) ds \\ &= \begin{cases} 4\pi^2 R^2 B^{HL} \frac{\sqrt{1+\varepsilon^2}}{\varepsilon} \mathcal{J}_1\left(\frac{R\pi}{L} |m|\right) / \left(\frac{R\pi}{L} |m|\right), & m \neq 0 \\ 2\pi^2 R^2 B^{HL} \frac{\sqrt{1+\varepsilon^2}}{\varepsilon}, & m = 0. \end{cases} \end{aligned}$$

**Step 3** Perform inverse Fourier transforms to approximate  $Q_\varepsilon^{LH}(v^L)$  and  $\tilde{Q}_\varepsilon^{HL}(\tilde{v}^H)$

**A.3. Fourier transforms for scaled functions.** While most of the process is straightforward, the main challenge arises from the numerical handling of the scaling  $f^H(v^H) = \varepsilon^{d_v} \tilde{f}^H(\tilde{v}^H)$ , where  $f^H$  is defined on the regular grid as specified in Section 3. Additionally, deriving  $Q_\varepsilon^{HL}(v^H)$  from  $\tilde{Q}_\varepsilon^{HL}(\tilde{v}^H)$  presents further complexity. Due to the scaling nature of the problem, a simple interpolation approach would offer limited effectiveness.

Our strategy, therefore, is to leverage the dilation property of Fourier transforms to handle the numerical rescaling more effectively. More specifically, by assuming that  $\tilde{f}^H(\tilde{v}^H)$  has support  $\mathcal{B}_{\varepsilon S}$ , we have by (A.1)

$$(A.5) \quad \hat{f}_m^H = \frac{1}{(2L)^{d_v}} \int_{\mathcal{D}_L} \tilde{f}^H(\tilde{v}^H) e^{-i\frac{\pi}{L} m \cdot \tilde{v}^H} d\tilde{v}^H = \frac{1}{(2L)^{d_v}} \int_{\mathcal{D}_L} f^H(v^H) e^{-i\frac{\pi}{L} \varepsilon m \cdot v^H} dv^H.$$

This way, we obtain the coefficients  $\{\hat{f}_m^H\}$  directly from an integration of  $f^H$ , without resorting to the numerical representation of  $\hat{f}^H$ .

Similarly, we can get  $Q^{HL}$  directly from  $\{\hat{Q}_{\varepsilon,k}^{HL}\}$  by

$$(A.6) \quad Q_\varepsilon^{HL}(f^H, f^L)(v^H) = \frac{\varepsilon^2}{(2L)^2} \sum_{k=-\frac{Nv}{2}}^{\frac{Nv}{2}-1} \hat{Q}_{\varepsilon,k}^{HL} e^{i\frac{\pi}{L}\varepsilon k \cdot v^H}.$$

**B. Derivation of asymptotic operators.** The derivation is based on the Taylor expansion of the integrand, following the collision rules given by (2.5) and (2.7)

$$f^L(v'^L) f^H(v^H) - f^L(v^L) f^H(v^H) = I_0 + \varepsilon I_1 + \varepsilon^2 I_2 + \mathcal{O}(\varepsilon^3),$$

where

$$\begin{aligned} I_0 &= \left( f^L(|v^L|\sigma) - f^L(v^L) \right) f^H(v^H), \\ I_1 &= f^L(|v^L|\sigma)(v^L - |v^L|\sigma) \cdot \nabla_{v^H} f^H(v^H) \\ &\quad + f^H(v^H)(v^H - \frac{(v^L \cdot v^H)}{|v^L|}\sigma) \cdot \nabla_{v^L} f^L(|v^L|\sigma), \end{aligned}$$

and

$$\begin{aligned} I_2 &= \frac{1}{2} f^L(|v^L|\sigma)(v^L - |v^L|\sigma)^{\otimes 2} : \nabla_{v^H}^2 f^H(v^H) \\ &\quad + f^L(|v^L|\sigma)(-v^H + \frac{(v^L \cdot v^H)}{|v^L|}\sigma) \cdot \nabla_{v^H} f^H(v^H) \\ &\quad + \frac{1}{2} f^H(v^H)(v^H - \frac{(v^L \cdot v^H)}{|v^L|}\sigma)^{\otimes 2} : \nabla_{v^L}^2 f^L(|v^L|\sigma) \\ &\quad + (v^H - \frac{(v^L \cdot v^H)}{|v^L|}\sigma) \cdot \nabla_{v^L} f^L(|v^L|\sigma)(v^L - |v^L|\sigma) \cdot \nabla_{v^H} f^H(v^H) \\ &\quad + f^H(v^H)(v^L + \frac{1}{2}|v^L|\sigma(\frac{|v^H|^2}{|v^L|^2} - \frac{(v^L \cdot v^H)^2}{|v^L|^4}) - |v^L|\sigma) \cdot \nabla_{v^L} f^L(|v^L|\sigma). \end{aligned}$$

To deal with the singularity at the origin, we let  $v^L = 0$  in (2.5), leading to  $I_0 = 0$  and

$$\begin{aligned} I_1 &= (v^H + |v^H|\sigma) \cdot \nabla_{v^L} f^L(0) f^H(v^H), \\ I_2 &= f^L(0)(-v^H - |v^H|\sigma) \cdot \nabla_{v^H} f^H(v^H). \end{aligned}$$

## References.

- [1] S. I. BRAGINSKII, *Transport Processes in a Plasma*, Rev Plasma Phys, 1 (1965), p. 205.
- [2] R. BRUN, ed., *High Temperature Phenomena in Shock Waves*, vol. 7 of Shock Wave Science and Technology Reference Library, Springer Berlin, Heidelberg, Berlin, Heidelberg, 1 ed., 2012.
- [3] C. CERCIGNANI, *The Boltzmann equation and its applications*, vol. 67 of Applied Mathematical Sciences, Springer-Verlag, New York, 1988.
- [4] C. CERCIGNANI, R. ILLNER, AND M. PULVIRENTI, *The mathematical theory of dilute gases*, vol. 106 of Applied Mathematical Sciences, Springer-Verlag, New York, 1994.
- [5] S. CHAPMAN AND T. COWLING, *The Mathematical Theory of Non-uniform Gases: An Account of the Kinetic Theory of Viscosity, Thermal Conduction and Diffusion in Gases*, Cambridge Mathematical Library, Cambridge University Press, 1990.

- [6] F. CHARLES AND L. DESVILLETES, *Small mass ratio limit of Boltzmann equations in the context of the study of evolution of dust particles in a rarefied atmosphere*, J. Stat. Phys., 137 (2009), pp. 539–567.
- [7] R. M. CHMIELESKI AND J. H. FERZIGER, *Transport Properties of a Nonequilibrium Partially Ionized Gas in a Magnetic Field*, Phys Fluids, 10 (1967), pp. 2520–2530.
- [8] P. DEGOND, *Chapter 1 - asymptotic continuum models for plasmas and disparate mass gaseous binary mixtures*, in Material Substructures in Complex Bodies, G. Capriz and P. M. Mariano, eds., Elsevier Science Ltd, Oxford, 2007, pp. 1–62.
- [9] P. DEGOND AND B. LUCQUIN-DESREUX, *The asymptotics of collision operators for two species of particles of disparate masses*, Math. Models Methods Appl. Sci., 6 (1996), pp. 405–436.
- [10] P. DEGOND AND B. LUCQUIN-DESREUX, *Transport coefficients of plasmas and disparate mass binary gases*, Transport Theory Statist. Phys., 25 (1996), pp. 595–633.
- [11] G. DIMARCO AND L. PARESCHI, *Numerical methods for kinetic equations*, Acta Numer., 23 (2014), pp. 369–520.
- [12] F. FILBET AND S. JIN, *A class of asymptotic-preserving schemes for kinetic equations and related problems with stiff sources*, J. Comput. Phys., 229 (2010), pp. 7625–7648.
- [13] F. FILBET, C. MOUHOT, AND L. PARESCHI, *Solving the Boltzmann equation in  $N \log_2 N$* , SIAM J. Sci. Comput., 28 (2006), pp. 1029–1053.
- [14] G. FOLLAND, *Fourier Analysis and Its Applications*, Pure and applied undergraduate texts, American Mathematical Society, 2009.
- [15] I. M. GAMBA AND J. R. HAACK, *A conservative spectral method for the Boltzmann equation with anisotropic scattering and the grazing collisions limit*, J. Comput. Phys., 270 (2014), pp. 40–57.
- [16] I. M. GAMBA, J. R. HAACK, C. D. HAUCK, AND J. HU, *A fast spectral method for the Boltzmann collision operator with general collision kernels*, SIAM J. Sci. Comput., 39 (2017), pp. B658–B674.
- [17] I. M. GAMBA, S. JIN, AND L. LIU, *Asymptotic-preserving schemes for two-species binary collisional kinetic system with disparate masses I: time discretization and asymptotic analysis*, Commun. Math. Sci., 17 (2019), pp. 1257–1289.
- [18] I. M. GAMBA, S. JIN, AND L. LIU, *Micro-macro decomposition based asymptotic-preserving numerical schemes and numerical moments conservation for collisional nonlinear kinetic equations*, J. Comput. Phys., 382 (2019), pp. 264–290.
- [19] E. GOLDMAN AND L. SIROVICH, *Equations for Gas Mixtures*, Phys Fluids, 10 (1967), pp. 1928–1940.
- [20] H. GRAD, *Rarefied gas dynamics*, in Rarefied Gas Dynamics, F. Devienne, ed., Pergamon Press, London, 1960, pp. 10–138.
- [21] S. JAISWAL, A. A. ALEXEENKO, AND J. HU, *A discontinuous Galerkin fast spectral method for the multi-species Boltzmann equation*, Comput. Methods Appl. Mech. Engrg., 352 (2019), pp. 56–84.
- [22] S. JAISWAL, J. HU, AND A. A. ALEXEENKO, *Fast deterministic solution of the full Boltzmann equation on graphics processing units*, AIP Conference Proceedings, 2132 (2019), p. 060001.
- [23] S. JIN, *Efficient asymptotic-preserving (AP) schemes for some multiscale kinetic equations*, SIAM J. Sci. Comput., 21 (1999), pp. 441–454.
- [24] S. JIN AND Q. LI, *A BGK-penalization-based asymptotic-preserving scheme for*

- the multispecies Boltzmann equation*, Numer. Methods Partial Differential Equations, 29 (2013), pp. 1056–1080.
- [25] S. JIN AND Y. SHI, *A micro-macro decomposition-based asymptotic-preserving scheme for the multispecies Boltzmann equation*, SIAM J. Sci. Comput., 31 (2009/10), pp. 4580–4606.
- [26] E. A. JOHNSON, *Energy and momentum equations for disparate-mass binary gases*, Phys Fluids, 16 (1973), pp. 45–49.
- [27] C. MOUHOT AND L. PARESCHI, *Fast algorithms for computing the Boltzmann collision operator*, Math. Comp., 75 (2006), pp. 1833–1852.
- [28] L. PARESCHI AND B. PERTHAME, *A Fourier spectral method for homogeneous Boltzmann equations*, in Proceedings of the Second International Workshop on Nonlinear Kinetic Theories and Mathematical Aspects of Hyperbolic Systems (Sanremo, 1994), vol. 25, 1996, pp. 369–382.
- [29] L. PARESCHI AND G. RUSSO, *Numerical solution of the Boltzmann equation. I. Spectrally accurate approximation of the collision operator*, SIAM J. Numer. Anal., 37 (2000), pp. 1217–1245.
- [30] J.-P. PETIT AND J.-S. DARROZES, *Une nouvelle formulation des équations du mouvement d'un gas ionisé dans un régime dominé par les collisions*, J. Mécanique, 14 (1975), pp. 745–759.
- [31] L. J. SPITZER AND R. HARM, *Transport phenomena in a completely ionized gas*, Phys Rev, 89 (1953), pp. 977–981.
- [32] W. T. TAITANO, L. CHACÓN, AND A. N. SIMAKOV, *An adaptive, conservative 0D-2V multispecies Rosenbluth-Fokker-Planck solver for arbitrarily disparate mass and temperature regimes*, J. Comput. Phys., 318 (2016), pp. 391–420.
- [33] K. TAKASE, *Three-dimensional numerical simulations of dust mobilization and air ingress characteristics in a fusion reactor during a lava event*, Fusion Eng. Des., 54 (2001), pp. 605–615.
- [34] S. TAKATA AND F. C. GOLSE, *Half-space problem of the nonlinear Boltzmann equation for weak evaporation and condensation of a binary mixture of vapors*, Eur. J. Mech. B Fluids, 26 (2007), pp. 105–131.
- [35] L. WU, J. ZHANG, J. M. REESE, AND Y. ZHANG, *A fast spectral method for the Boltzmann equation for monatomic gas mixtures*, J. Comput. Phys., 298 (2015), pp. 602–621.
- [36] B. YAN AND S. JIN, *A successive penalty-based asymptotic-preserving scheme for kinetic equations*, SIAM J. Sci. Comput., 35 (2013), pp. A150–A172.